Investigation of variable aeration of monodisperse mixtures: implications for Pyroclastic Density Currents

Gregory M. Smith • Rebecca Williams • Pete J. Rowley • Daniel R. Parsons
School of Environmental Sciences, University of Hull, Hull, HU6 7RX, United Kingdom
e-mail: Gregory.Smith@2016.hull.ac.uk

High gas pore pressures are known to be important in dense pyroclastic density currents (PDCs), causing the flows to be highly mobile. However, the influence of spatial and temporal variations in pore pressure within PDCs has yet to be investigated. Theory suggests that variability in the fluidisation and aeration of a current will have a significant control on PDC flow and deposition. Here, the effect of spatially heterogeneous gas pore pressures in experimental PDCs was investigated. Sustained, unsteady granular flows were released into a flume channel where the injection of gas through the channel base was controlled to create spatial variations in aeration. Maximum flow front velocity is achieved by high degrees of aeration proximal to the source, rather than lower sustained aeration along the whole flume channel. However, moderate aeration (i.e. ~0.5 minimum static fluidisation velocity (U_{mf_st})) sustained throughout the propagation length of a flow results in greater runout distances than flows closer to fluidisation (i.e. 0.9 U_{mf_st}) near to source then de-aerating

distally. Additionally, although all aerated flows are sensitive to channel base slope angle, the runout distance of those flows where aeration is sustained throughout the length of the flow increase by up to 54% with an increase of slope from 2° to 4°. Deposit morphologies are primarily controlled by the spatial differences in aeration; where there is large decrease in aeration the flow forms a thick depositional wedge. Sustained gas-aerated granular currents are observed to be spontaneously unsteady, with internal sediment waves travelling at different velocities.

Keywords Fluidisation • Pyroclastic density current • Flume • Pore pressure • Slope angle • Aerated currents

Acknowledgements This work was carried out as part of a PhD project funded by a University of Hull PhD scholarship in the Catastrophic Flows Research Cluster. Experiments were performed in the Geohazards Lab at the University of Portsmouth, using equipment funded by a British Society for Geomorphology Early Career Researcher Grant held by PR. We thank two anonymous reviewers, whose comments and suggestions significantly improved this manuscript.

Introduction

Pyroclastic Density Currents (PDCs) are hazardous flows of hot, density driven mixtures of gas and volcanic particles formed during explosive volcanic eruptions, or from the collapse of lava domes. They are capable of depositing large ignimbrite sheets, which can exhibit a variety of sedimentary structures (e.g. Branney & Kokelaar, 2002; Brown & Branney, 2004). PDC transport encompasses a spectrum whose end-members are defined as either fully dilute flows or granular-fluid flows (Branney & Kokelaar, 2002; Breard & Lube, 2016). In the first type, clast interactions are negligible, and support and transport of the pyroclasts is dominated by fluid turbulence at all levels of the current. In contrast, granular-fluid based currents comprise concentrated flows where particle interactions are important and turbulence is dampened. Here, the differential motion between the interstitial gas and solid particles is able to generate pore fluid pressure due to the relatively low permeability of the gas-particle mixture. An intermediate regime has also recently been defined, characterised by mesoscale turbulence clusters (Breard et al. 2016), which couple the dilute and dense regions of a PDC.

PDCs can achieve long runout distances on slopes shallower than the angle of rest of granular materials, even at low volumes (e.g. Druitt et al. 2002; Cas et al. 2011; Roche et al. 2016). This high mobility is commonly attributed to the influence of fluidisation of the current's particles caused by high, long-lived gas pore pressures (Sparks, 1976; Wilson, 1980; Druitt et al. 2007; Roche, 2012, Gueugneau et al. 2017, Breard et al. 2018). These high gas pore pressures fundamentally result from relative motion between settling particles and ascending fluid, and can be produced through various processes including (i) flow fluidisation; (ii) bulk self-fluidisation; (iii) grain self-fluidisation; and (iv) sedimentation fluidisation; see Wilson (1980) and Branney & Kokelaar (2002) for reviews.

As gas pore pressures within a gas-particle mixture increase, inter-particle stresses are reduced as the particles become fluidised (Gibilaro et al. 2006, Roche et al. 2010).

Fluidisation of a granular material is defined as the condition where a vertical drag force exerted by a gas flux is strong enough to support the weight of the particles, resulting in apparent friction reduction and fluid-like behaviour (Druitt et al. 2007; Gilbertson et al. 2008). The gas velocity at which this occurs is known as the minimum fluidisation velocity(U_{mf}). Where there is a gas flux through a sediment which is less than U_{mf}, then that sediment flow is partially-fluidised and is often termed aerated.

The gas pore pressure is known to decrease over time during a flow, after it is created and there is little or no relative gas-particle motion, according to:

$$\mathrm{t}_d \propto \mathrm{H}^2/D$$

Where H is the bed height and D is the diffusion coefficient of the gas (Roche, 2012). PDCs are dominated by finer-grained particles, which confer a greater surface area than coarse particles, conveying low mixture permeability (Druitt et al. 2007; Roche, 2012). PDCs are therefore thought to be able to sustain high pore pressures for longer, resulting in greater mobility than their dry granular counterparts.

The detailed fluid dynamics and processes involved in the changes and fluxes involved in PDC pore pressure are, however, elusive given the significant challenge and difficulty in obtaining measurement of such hostile flows. Moreover, the ability to observe depositional processes in action would be challenging as the basal parts of PDCs are hidden by an overriding ash cloud. Scaled, physical modelling, however, provides a direct way to simulate and quantify the behaviour of several processes which take place in PDCs under controlled, variable conditions, as well as creating easily accessible deposits which may be analogous to their natural counterparts.

Experimental dam-break type flows aimed at representing simplified, uniformly permeable, dense PDCs have attempted to model fluidisation processes by fluidising particles before release into a flume (e.g. Roche et al. 2002; Roche et al. 2004). This demonstrated that fluidisation had an important effect on runout distance. However, rapid pore-pressure diffusion resulted in shorter runout distances and thinner deposits than might be expected in full scale flows e.g. (Roche et al. 2004; Girolami et al. 2008; Roche et al. 2010; Roche, 2012; Montserrat et al. 2016). This is because while the material permeability in both natural and experimental flows is similar (with experimental flows somewhat fines depleted in comparison to natural PDCs), experimental flows are much thinner than their natural counterparts, resulting in their more rapid loss of pore-pressure. Early work on the sustained fluidisation of granular currents by injection of air at the base of the flow (e.g. Eames & Gilbertson, 2000) was not focused on replicating the behaviour of PDCs in particular, but did demonstrate that this was a valid method of preventing rapid pore-pressure diffusion in granular currents. Rowley et al. (2014) reproduced the long-lived high gas pore pressures of sustained PDCs using an experimental flume which fed a gas flux through a porous basal plate to simulate long pore pressure diffusion timescales in natural, thicker flows. This resulted in much greater runout distances than unaerated or initially fluidised currents, however, these experiments were unable to explore defluidisation due to the constant uniform gas supply along the flume length. This work simulates PDCs with spatial variations in pore pressure, and begins to explore their response to slope angle. This is important because natural PDCs are unlikely to be laterally homogenous in aeration, (Gueugneau et al. 2017) - they are inherently heterogeneous due to factors such as source unsteadiness and segregation of particles (Branney & Kokelaar, 2002), which can cause spatial variability in factors controlling U_{mfst}, such as bulk density. Hence, different pore pressure generation mechanisms may be operating in different areas of the PDC at once. For example, fluidisation due to the exsolution of volatiles from juvenile clasts (Sparks, 1978; Wilson, 1980) could be dominant in one part of the PDC, fluidisation from hindered settling of depositing particles (Druitt, 1995; Girolami et al. 2008) or autofluidisation from particles settling into substrate interstices (Chédeville & Roche, 2014), dominant in another . It is important, then, to understand the impacts of variable fluidisation on such flows. It should be noted that our work attempts to simulate the fact that PDCs are fluidised/aerated to some degree for long periods of time, rather attempting to replicate a particular mechanism of fluidisation.

Here we present experiments using a novel flume tank which can investigate the effect of spatially variable aeration on a sustained granular current at different points in its propagation. The flume allows the simulation of various pore pressures and states of aeration in the same current along the channel. This allows the flows to stabilise and propagate for a controlled distance before defluidisation occurs. We report how this spatially variable aeration, as well as the channel slope angle, affects the flow runout distance, frontal velocity, and characteristics of the subsequent deposit.

Methods

The experimental flume is shown in Fig. 1. A hopper supplies the particles to a 0.15 m wide 3.0 m long channel through a horizontal lock gate 0.64 m above the channel base. The base of the flume sits above three 1.0 m long chambers, each with an independently controlled compressed air supply, which feeds into the flume through a porous plate. The flume channel can be tilted up to 10 degrees from horizontal.

The air-supply plumbing allows a gas flux to be fed through the base of the flume, producing sustained aeration of the flow. In such thin (<30 mm), rapidly degassing laboratory flows this enables us to simulate the long-lived high gas pore pressures that characterize thicker PDCs (Rowley et al. 2014). The novel aspect of this flume is that the gas flux for each of the three chambers may be controlled individually, allowing the simulation of spatially variable magnitudes of pore pressures.

The experiments were performed using spherical soda lime ballotini with grain sizes of 45-90 µm (average D_{32} = 63.4 µm calculated from six samples across the material batch, see Appendix A for grain size information), similar to the type of particles used in previous experimental granular currents (e.g. Roche et al. 2004; Rowley et al. 2014; Montserrat et al. 2016). D_{32}, or the Sauter mean diameter, can be expressed as

$$D_{32} = \frac{1}{\Sigma \frac{x_i}{d_i}}$$

Where x_i is the weight fraction of particles of size d_i. In line with Breard et al. (2018), D_{32} was given here because it exerts some control on flow permeability (Li & Ma 2011).

These grain sizes assign the ballotini to the Group A of Geldart (1973), which are those materials which expand homogenously above U_{mf} until bubbles form. As PDCs contain dominantly Group A particles, this allows dynamic similarity between the natural and experimental flows (Roche, 2012). The ballotini have a solid density of 2500 kg/m^3 and a repose angle of 27°.

The experiments were recorded using high-speed video at 200 frames per second. This video recorded a side-wall area of the channel across the first and second chambers, allowing the calculation of variations in the flow front velocity. All runout measurements are given as a distance from the headwall of the flume.

The variables experimentally controlled, and thus investigated, in these experiments are: (i) the gas flux supplied through the base in each of the three sections of the channel, and (ii) the slope angle of the channel. The slope angles examined were 2° and 4°. A range of gas supply velocities were used to vary the aeration state of the particles, all of which were below U_{mf} as complete fluidisation would result in non-deposition. Static piles of particles used in these experiments achieve static minimum fluidisation (U_{mf_st}) with a vertical gas velocity of 0.83 cm/s, comparable to Roche (2012), who used the same 45-90 µm glass ballotini. Because our fluidisation state was measured in a static pile, we explicitly use U_{mf_st} rather than U_{mf} in order to denote the origin of this value in these experiments. In a moving (i.e. shearing) flow U_{mf} will be higher than U_{mf_st} because dilatancy would be anticipated, and therefore an increase in porosity should be observed.

Aeration states were varied from 0 cm/s (non-aerated) through various levels of aeration to a maximum of 0.77 cm/s. Table 1 shows the gas velocities used as a proportion of U_{mf_st} across the experimental set. When describing the aeration state of the flume as a whole, the gas velocities of each chamber are listed as proportions of U_{mf_st}, in increasing distance from the headwall. The mass of particles comprising the flows (the "charge") was kept constant, at 10 kg for each run.

Results

Runout distance and flow front velocity

Runout distance is markedly affected by variations in the aeration states. For a given slope angle, if the aeration states are the same in all three chambers, then increasing the gas flux causes runout distances to increase. The measurable limit in these experiments is 3 m (i.e. when the flow exits the flume) (Fig. 2).

Where aeration state is decreased along the length of the flume, greater runout distances are still correlated with greater aeration states. At a high aeration state in the first chamber behaviour of the flow is dependent on the aeration state in the second chamber. For example Fig. 2 demonstrates how 0.93-0.93-0 U_{mf_st} flows have a greater runout distance than 0.93-0.66-0 U_{mf_st} flows which in turn have a greater runout distance than 0.93-0-0 U_{mf_st} flows. At a lower aeration state in the first chamber the runout distance seems to be dependent on the aeration state in the third chamber. For example, in Fig. 2 0.66-0.53-0.4 U_{mf_st} flows have a greater runout distance than 0.66-0.66-0 U_{mf_st} flows and 0.53-0.4-0.4 U_{mf_st} flows have a greater runout distance than 0.53-0.53-0 U_{mf_st} flows.

The flow front velocity is also dependent on the aeration state. Velocities were calculated at 0.1 m intervals, from high-speed video which recorded the currents across a section of the flume from 0.8 to 1.7 m. Flow front velocity does not exceed 1.5 m/s (Fig. 3). This is considerably less than the calculated free fall velocity $(2gh)^{1/2}$ = 3.5 m/s, where h = the 0.64 m drop height, however by the interval at which velocity is measured the flows have travelled 0.8 m and will also have lost energy upon impingement. Generally, regardless of the aeration state in the first or second chamber, the flow front velocity decreases over the measured interval (Fig. 3). Higher aeration states, however, sustain higher flow front velocities across greater distances. Also, where the aeration state decreases from the first chamber into the second, the flow front velocity is not always immediately affected, and may even temporarily increase (Fig. 3). Overall, the highest flow front velocities across the whole 0.9 m interval are always found in the 0.93-0.93-0 U_{mf_st} aeration state.

Slope angle and runout distance

For a given aeration state, increasing the slope angle acts to increase the runout distance of the flow (Fig. 2).

However, the magnitude of the increase is dependent on the overall aeration state of the flow; large increases in runout distance from increased slope angle only occur where the flow is uniformly aerated or there is a small decrease in gas flux between chambers. For example, 0.4-0.4-0.4 U_{mf_st}, 0.46-0.46-0.46 U_{mf_st}, and 0.53-0.4-0.4 U_{mf_st} flows see increases in runout distances from 1.3 m to 2 m (54%), 2 to 3+ m (≥50%), and 2 m to 2.43 m (22%) respectively, on a 2° slope compared to a 4° slope. Whether this is also the case for higher uniformly aerated states (0.53-0.53-0.53 U_{mf_st} and 0.66-0.66-0.66 U_{mf_st}) is not clear as here both slope angles result in maximum flow runout.

The effect of increasing slope angle on increasing runout distance is subdued when flows are allowed to de-aerate more quickly. For example, flows under of 0.93-0.66-0 U_{mf_st} only experience a runout increase from 2.53 m to 2.86 m (13%) between 2-4°, while 0.93-0-0 conditions see increases of 2.88 m to 3+ m (≥6%).

Slope angle is thus a secondary control on runout distance compared to aeration state. Only in one condition does increasing the slope by 2° increase the runout distance by more than 50% (1.3 m to 2 m), whereas on a 2° slope, increasing aeration from zero to just 0.4-0.4-0.4 U_{mf_st} results in a 120% increase in runout distance (0.59 m to 1.3 m). Increasing this to the maximum aeration state used, 0.93-0.93-0 U_{mf_st}, gives a further increase in runout distance of 122% (1.3 m to 2.88 m).

Flow behaviour and deposition

Regardless of aeration state, all of the experimental flows appear unsteady. This is manifested in the transport of the particles as a series of pulses, not always laterally continuous, wherein slower, thinner pulses at the flow front are overtaken by faster, thicker pulses. This can partly be seen in the waxing and waning of the velocity profiles in Fig. 3; some of the fluctuations in flow front velocity are caused by a faster flow pulse reaching the front of the flow (Fig. 4). However, in most cases the overtaking of the first pulse happens outside the area of the high-speed camera, and appears to be triggered by the flow front slowing as it transitions into a less aerated chamber.

There appears to be five different populations of deposit morphology types generated by the various combinations of aeration states and slope angles (Table 2):

- *Large aeration decrease* - In cases where the flow front passes into an unaerated chamber from a chamber that is aerated at 0.93 U_{mf_st} (i.e. almost U_{mf_st}), the resulting deposit is mostly confined to the unaerated chamber in a wedge shape, with its thickest point being the transition between the highly aerated and completely unaerated chambers. Such behaviour is also seen in the aeration state 0.93-0.66-0 U_{mf_st}, most clearly on a 4° slope.
- *Uniform aeration* - Where all three chambers are aerated at 0.53 U_{mf_st} or above, the flow reaches the end of the flume. Except for flows passing through all

chambers at 0.66 U_{mf_st}, the flows forming these deposits experience stalling of the flow front, which then progresses at a much slower rate while local thickening along the body of the flow results in deposition upstream. The section of the deposit in the third chamber is usually noticeably thinner than its bulk, which tends to be of an even thickness. Such deposits are also formed by 0.46-0.46-0.46 U_{mf_st} flows on a 4° slope.

- *Moderate – low aeration decrease* - Where the gas fluxes in the first two chambers are at 0.66 U_{mf_st} or 0.53 U_{mf_st} but there is no (or low) flux in the third, the deposits formed are of approximately even thicknesses, with their leading edges inside the third chamber. This family could also include deposits formed under 0.93-0.66-0 U_{mf_st} conditions on a 2° slope.
- *Low uniform aeration* - Where the second and third chambers are aerated at 0.46 U_{mf_st} or less and the first chamber at no more than 0.53 U_{mf_st}, deposits with a centre of mass located inside the first chamber form; beyond this the deposit thicknesses decreases rapidly.
- *Unaerated* Under no aeration whatsoever, deposits form flat-topped wedges. These show angles steeper than the wedges in other populations.

Discussion

Runout distance

Once the flow is fluidised or aerated it is able to travel further than dry granular currents, as seen in previous experiments (e.g. Roche et al. 2004; Girolami et al. 2008; Roche, 2012; Chédeville & Roche, 2014; Rowley et al. 2014; Montserrat et al. 2016). This is because the increased pore pressures reduce frictional forces between the particles in the flow, thus increasing mobility. However, here the relationship between aeration state and runout distance is not a simple correlation between higher gas fluxes and longer runout distances. A flow with high initial aeration rates followed by a rapid decline does not travel as far as a flow moderately aerated across a greater distance. For example, a flow run with 0.93-0-0 U_{mf_st} conditions does not travel as far as runs with conditions set at 0.66-0.66-0.66 U_{mf_st} or 0.53-0.53-0.53 U_{mf_st} (Fig. 2).

A highly aerated flow may continue on for some distance after passing into an unaerated chamber. Where the unaerated chamber is the final one, this distance is more dependent on the aeration state of the first chamber than the second. For example, a flow under 0.93-0.66-0 U_{mf_st} conditions travels up to 24% further than one under 0.66-0.66-0 U_{mf_st} conditions, but a flow under 0.93-0.93-0 U_{mf_st} conditions only travels up to 14% further than one under 0.93-0.66-0 U_{mf_st} conditions. However, a flow that is moderately aerated for its entire passage can travel at least as far as those which are initially highly aerated. This is a result of the high pore pressures being sustained across a longer portion of the flow, simulating the long-lived high pore pressures of much thicker natural PDCs. Where a flow passes into an unaerated chamber, the pore pressure diffusion time is dependent on the flow thickness, flow permeability, and the current pore pressure magnitude. As many flow fronts are of similar thickness when they pass into an unaerated chamber, de-aeration seems to be controlled largely by the aeration state of the chambers prior to the unaerated one. A flow with a lower aeration state will reach a completely de-aerated state and halt sooner than a flow with a higher aeration state. This has implications for both runout distance and deposit characteristics.

Velocity

Higher initial gas velocities sustain higher flow front velocities for longer, as seen in Fig. 3, where the 0.93-0.93-0 U_{mf_st} and 0.93-0.66-0 U_{mf_st} flow velocity profiles sustain flow front velocities of >1 m/s across the measured interval, in contrast to the other aeration states, where flow front velocities rapidly fall below 1 m/s. High gas fluxes sustain high pore pressures, decreasing frictional forces between particles, reducing deceleration relative to less aerated currents. As the rate of pore pressure diffusion becomes greater than the supply of new gas to the flow it undergoes an increase in internal frictional forces and consequent decrease in velocity.

When a flow crosses into a chamber with a lower aeration state, this results in the lowering of its flow front velocity (Fig. 3), although this change does not immediately take place and the flow front may even accelerate as it crosses the boundary (e.g. many profiles in Fig. 3). The only flows which immediately decelerate in all cases are those where the aeration state of both chambers is 0.53 U_{mf_st} or less. The temporary acceleration seen in the other flows mostly occurs over a distance of ~10 cm. There, these flows have sufficient momentums that the decreasing gas velocity and consequent increase in internal frictional forces does not immediately take effect.

This is in line with our knowledge of pore pressure diffusion in PDCs – mostly comprised of fine ash, the pore pressure does not instantly diffuse due to the low permeability of the material (e.g. Druitt et al. 2007). In these experimental flows, passing into a lower or non-aerated chamber does not cause the flow to immediately lose pore pressure (Fig. 3), but the magnitude of the difference in gas velocities between the chambers does influence the depositional behaviour of the flow.

The influence of slope angle

The effects of slope angle on both dam-break type initially fluidised (Chédeville & Roche, 2015) and dry granular flows (Farin et al. 2014) are relatively well known. However the influence of varying slope angle for flows possessing sustained pore pressures is largely unquantified. Although only two (2° and 4°) slope angles were examined, there is a clear effect on both flow runout distance and flow front velocity. Runout distance may be increased by up to 50% and higher flow front velocities are sustained for longer on a steeper slope. The influence of small changes of slope on PDC dynamics is important because in nature low slope angles can nevertheless cause PDC runout distances >100 km (e.g. Valentine et al. 1989; Wilson et al. 1995).

The effect of slope angle on runout distance is most apparent when aeration is sustained over the whole flow. Where the flow front comes to a halt in an unaerated chamber, the runout distance increases no more than 13% on a 4° slope compared to a 2° slope. However, the overall effect of slope angle on the runout distance of sustained, moderate to highly aerated currents is difficult to quantify as these commonly run out of the flume.

Deposit formation

These experimental flows travel as a series of pulses generated by inherent unsteadiness developed during flow propagation. Froude numbers $Fr = \frac{U}{(gh)^{1/2}}$ were determined for a number of flow fronts and pulses by plotting the flow or pulse velocity as a function of $(gh)^{\frac{1}{2}}$ (Fig. 5). The slope of line of best fit gives Fr = 7, which fits with anticipated supercritical flow conditions (Gray et al. 2003). This is higher that the Fr = 2.58 obtained by Roche et al. (2004), likely due to the higher energy initiation and sustained nature of our flows compared to their depletive, dam-break currents.

The flows form a range of depositional structures depending on the flow dynamics and can deposit, through aggradation, much thicker deposits than the flows themselves. The deposits produced in the experiments can be grouped into five different populations; from which the following important observations can be made: (1) Where the flow front moves from an aerated chamber into an unaerated one, the shape and thickness of the deposit appears to depend on the magnitude of the drop in aeration state. Where the drop is high (0.93 U_{mf_st} and 0.66 U_{mf_st} to unaerated) - a thick (~ x10 flow thickness) wedge forms downstream, thickening mainly through retrogradational deposition as the high aeration states of the first two chambers quickly deliver the flow body into the growing wedge.; (2) Sustained flow can build a relatively even thickness deposit behind a stalling flow front (e.g Williams et al. 2014); and (3) Flat-topped wedges form where flows are dry and runout distance is therefore affected only by channel slope angle. Overall these results suggest that a decrease in aeration state may be an important control on deposit formation, character, and distribution. These experiments provide a first attempt to directly control de-aeration in dense granular PDC analogues, and greatly simplify the system, providing three relatively uniformly aerated segments of flow. This is in contrast to the high degree of spatial and temporal variation that might be envisaged in PDCs, and the more gradual degassing a natural current will experience. We would highlight that the de-aeration rates observed in these experiments are faster than we would anticipate in natural PDCs; the sustained gas pore pressure provided here is specifically to overcome the very rapid pore pressure diffusion timescales found in laboratory flows which have similar or larger grainsizes to the ash found in PDCs. Still, the rapid decreases in aeration seen in some of our experimental flows could be analogous to PDCs which may experience de-aeration processes. These might include (1) a sudden loss of fines, (2) flow thinning, (3) a drop in temperature, (4) entrainment of heterogeneous material, or (5) an increase in shear dilatancy (e.g. Bareschino et al. 2007, Druitt et al. 2007, Gueugneau et al. 2017). While these experiments give flow height to de-aeration length-scale ratios in the order of 0.1-0.01 (1 cm thick flows de-aerating over 10's of cm) in PDCs we would anticipate ratios in the order of 0.001 such that meter thick flows defluidise over 100's to 1000's of metres.

Implications for future work

We have demonstrated that variable aeration states in conjunction with slope angle can affect the shape and location of an experimental flow's deposit. It seems logical to assume that these different styles of deposit aggrade differently and so have different internal architectures, which may be analogous to features seen in ignimbrites. However, the internal architectures of these experimental deposits are hidden due to the uniform colour and grain size of the particles used. In future work, the use of dyed particles or particles of a different size would help identify the internal features of these deposits.

Conclusions

These experiments examined granular flows with sustained and reducing pore pressures along inclined slopes. The flume configuration allowed the simulation of different aeration states within the flows, in order to simulate the dynamics and heterogeneous nature of pore pressure in pyroclastic density currents. We examined the effects of varying combinations of aeration states, as well as the effect of slope angle on flow field dynamics and deposit characteristics.

It is clear that, in a general sense, higher gas fluxes (higher pore pressures) in the flume chambers result in longer runout distances, but moderate (0.53 U_{mf_st} – 0.66 U_{mf_st}) sustained gas fluxes produce at least equal runouts to high (0.93 U_{mf_st}) initial fluxes that are subsequently declined. Similarly, high fluxes sustain higher flow front velocities for longer, and flows may travel for 0.1 m – 0.2 m after experiencing a decrease in gas flux supplied to their base before undergoing the consequent decrease in flow front velocity.

Slope angle variation between 2° and 4° has a measurable impact on flow runout distance, resulting in increases of between 0.11 m and 1 m, with greater increases where low (0.4 U_{mf_st} – 0.46 U_{mf_st}) levels of aeration are sustained for the whole runout distance of the flow. A higher slope angle also sustains higher flow front velocities for longer.

Finally, the findings also demonstrate intricate links between the overall flow dynamics and the deposit morphology characteristics, with thicker, more confined deposits aggrading rapidly where the flow transitions from a high aeration state to lower aeration states.

References

Bareschino, P., Gravina, T., Lirer, L., Marzocchella, A., Petrosino, P., Salatino, P. (2007) Fluidization and de-aeration of pyroclastic mixtures: The influence of fines content, polydispersity and shear flow. Journal of Volcanology and Geothermal Research, 164, 284-292. https://doi.org/10.1016/j.jvolgeores.2007.05.013

Branney, M. J., & Kokelaar, P. (2002). Pyroclastic Density Currents and the Sedimentation of Ignimbrites. Geological Society, London, Memoirs, 27(June 2007). https://doi.org/10.1144/GSL.MEM.2003.027.01.02

Breard, E. C. P., & Lube, G. (2016). Inside pyroclastic density currents – uncovering the enigmatic flow structure and transport behaviour in large-scale experiments. Earth and Planetary Science Letters, 1, 1–15. https://doi.org/10.1016/j.epsl.2016.10.016

Breard, E. C. P., Lube, G., Jones, J. R., Dufek, J., Cronin, S. J., Valentine, G., & Moebis, A. (2016). Coupling of turbulent and non-turbulent flow regimes within pyroclastic density currents. Nature Geoscience, 9, 767-771. https://doi.org/10.1038/ngeo2794

Breard, E. C. P., Dufek, J., & Lube, G. (2018). Enhanced mobility in concentrated pyroclastic density currents: An examination of a self-fluidization mechanism. Geophysical Research Letters, 45. https://doi.org/10.1002/2017GL075759

Brown, R. J., & Branney, M. J. (2004). Bypassing and diachronous deposition from density currents: Evidence from a giant regressive bed form in the Poris ignimbrite, Tenerife, Canary Islands. Geology, 32(5), 445-448. https://doi.org/10.1130/G20188.1

Cas, R. A. F., Wright, H. M. N., Folkes, C. B., Lesti, C., Porreca, M., Giordano, G., & Viramonte, J. G. (2011). The flow dynamics of an extremely large volume pyroclastic flow, the 2.08-Ma Cerro Galán Ignimbrite, NW Argentina, and comparison with other flow types. Bulletin of Volcanology, 73(10), 1583–1609. https://doi.org/10.1007/s00445-011-0564-y

Chédeville, C., & Roche, O. (2014). Autofluidization of pyroclastic flows propagating on rough substrates as shown by laboratory experiments. Journal of Geophysical Research: Solid Earth, (119), 1764–1776. https://doi.org/10.1002/2013JB010554

Chédeville, C., & Roche, O. (2015). Influence of slope angle on pore pressure generation and kinematics of pyroclastic flows: insights from laboratory experiments. Bulletin of Volcanology, 77(11), 1–13. https://doi.org/10.1007/s00445-015-0981-4

Druitt, T. H. (1995). Settling behaviour of concentrated dispersions and some volcanological applications. Journal of Volcanology and Geothermal Research, 65(1–2), 27–39. https://doi.org/10.1016/0377-0273(94)00090-4

Druitt, T. H., Calder, E. S., Cole, P. D., Hoblitt, R. S., Loughlin, S. C., Norton, G. E., Ritchie, R., Sparks, S. J., & Voight, B. (2002). Small-volume, highly mobile pyroclastic flows formed by rapid sedimentation from pyroclastic surges at Soufrière Hills Volcano, Montserrat: an important volcanic hazard. In: Druitt, T. H., & Kokelaar, B. P. (eds). The Eruption of Soufrière Hills Volcano, Montserrat, from 1995 to 1999. Geological Society, London, Memoirs, 21. 263-279. https://doi.org/10.1144/GSL.MEM.2002.021.01.12.

Druitt, T. H., Avard, G., Bruni, G., Lettieri, P., & Maez, F. (2007). Gas retention in fine-grained pyroclastic flow materials at high temperatures. Bulletin of Volcanology, 69(8), 881–901. https://doi.org/10.1007/s00445-007-0116-7

Eames, I., & Gilbertson, M. (2000). Aerated granular flow over a horizontal rigid surface. Journal of Fluid Mechanics, 424(November 2000), 169–195. https://doi.org/10.1017/S0022112000001920

Farin, M., Mangeney, A., & Roche, O. (2014). Fundamental changes of granular flow dynamics, deposition, and erosion processes at high slope angles: Insights from laboratory experiments. Journal of Geophysical Research: Earth Surface, 119(3), 504–532. https://doi.org/10.1002/2013JF002750

Geldart, D. (1973). Types of gas fluidization. Powder Technology, 7(5), 285–292. https://doi.org/10.1016/0032-5910(73)80037-3

Gibilaro, L. G., Gallucci, K., Di Felice, R., & Pagliai, P. (2007). On the apparent viscosity of a fluidized bed. Chemical Engineering Science, 62(1-2), 294-300. https://doi.org/10.1016/j.ces.2006.08.030.

Gilbertson, M. A., Jessop, D. E., & Hogg, A. J. (2008). The effects of gas flow on granular currents. Philosophical Transactions. Series A, Mathematical, Physical, and Engineering Sciences, 366(1873), 2191–203. https://doi.org/10.1098/rsta.2007.0021

Girolami, L., Druitt, T. H., Roche, O., & Khrabrykh, Z. (2008). Propagation and hindered settling of laboratory ash flows. Journal of Geophysical Research: Solid Earth, 113(2), 1–13. https://doi.org/10.1029/2007JB005074

Gray, J. M. N. T., Tai, Y.-C., & Noelle, S. (2003). Shock waves, dead zones and particle-free regions in rapid granular free-surface flows. Journal of Fluid Mechanics, 291, 161-181. https://doi.org/10.1017/S0022112003005317

Gueugneau, V., Kelfoun, K., Roche, O., & Chupin, L. (2017). Effects of pore pressure in pyroclastic flows : Numerical simulation and experimental validation. Geophysical Research Letters, 44, 2194-2202. https://doi.org/10.1002/2017GL072591.

Li, L., & Ma, W. (2011). Experimental study on the effective particle diameter of a packed bed with non-spherical particles. Transport in Porous Media, 89(1), 35-48. https://doi.org/10.1007/s11242-011-9757-2.

Montserrat, S., Tamburrino, A., Roche, O., Niño, Y., & Ihle, C. F. (2016). Enhanced run-out of dam-break granular flows caused by initial fluidization and initial material expansion. Granular Matter, 18(1), 1–9. https://doi.org/10.1007/s10035-016-0604-6

Roche, O. (2012). Depositional processes and gas pore pressure in pyroclastic flows: An experimental perspective. Bulletin of Volcanology, 74(8), 1807–1820. https://doi.org/10.1007/s00445-012-0639-4

Roche, O., Gilbertson, M. A., Phillips, J. C., & Sparks, R. S. J. (2002). Experiments on deaerating granular flows and implications for pyroclastic flow mobility. Geophysical Research Letters, 29(16), 1–4. https://doi.org/10.1029/2002GL014819

Roche, O., Gilbertson, M. A., Phillips, J. C., & Sparks, R. S. J. (2004). Experimental study of gas-fluidized granular flows with implications for pyroclastic flow emplacement. Journal of Geophysical Research B: Solid Earth, 109(10), 1–14. https://doi.org/10.1029/2003JB002916

Roche, O., Montserrat, S., Niño, Y., & Tamburrino, A. (2010). Pore fluid pressure and internal kinematics of gravitational laboratory air-particle flows: Insights into the emplacement dynamics of pyroclastic flows. Journal of Geophysical Research: Solid Earth, 115(9), 1–18. https://doi.org/10.1029/2009JB007133

Roche, O., Buesch, D. C., & Valentine, G. A. (2016). Slow-moving and far-travelled dense pyroclastic flows during the Peach Spring super-eruption. Nature Communications, 7. https://doi.org/10.1038/ncomms10890.

Rowley, P. J., Roche, O., Druitt, T. H., & Cas, R. (2014). Experimental study of dense pyroclastic density currents using sustained, gas-fluidized granular flows. Bulletin of Volcanology, 76(9), 1–13. https://doi.org/10.1007/s00445-014-0855-1

Sparks, R. S. J. (1976). Grain size variations in ignimbrites and implications for the transport of pyroclastic flows. Sedimentology, 23(2), 147–188. https://doi.org/10.1111/j.1365-3091.1976.tb00045.x

Sparks, R. S. J. (1978). Gas release rates from pyroclastic flows: a assessment of the role of fluidisation in their emplacement. Bulletin Volcanologique, 41(1), 1–9. https://doi.org/10.1007/BF02597679

Valentine, G. A., Buesch, D. C., & Fisher, R. V. (1989). Basal layered deposits of the Peach Springs Tuff, northwestern Arizona, USA. Bulletin of Volcanology, 51(6), 395–414. https://doi.org/10.1007/BF01078808

Williams, R., Branney, M. J., & Barry, T. L. (2014). Temporal and spatial evolution of a waxing then waning catastrophic density current revealed by chemical mapping. Geology. https://doi.org/10.1130/G34830.1

Wilson, C. J. N. (1980). The role of fluidization in the emplacement of pyroclastic flows: An experimental approach. Journal of Volcanology and Geothermal Research, 8(2–4), 231–249. https://doi.org/10.1016/0377-0273(80)90106-7

Wilson, C. J. N., Houghton, B. F., Kamp, P. J. J., & McWilliams, M. O. (1995). An Exceptionally Widespread Ignimbrite with Implications for Pyroclastic Flow Emplacement. Nature, 378(6557), 605–607. https://doi.org/10.1038/378605a0

Appendix A

[Table 3]

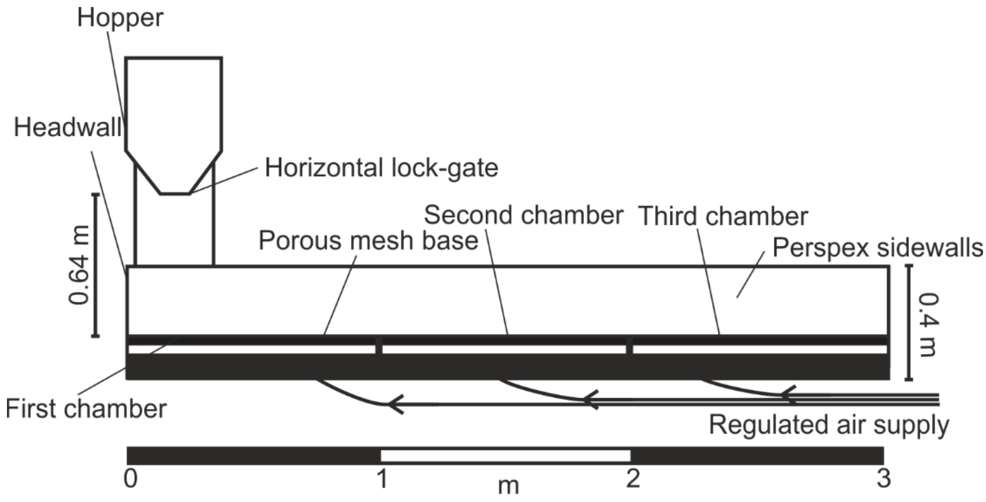

Fig. 1 A longitudinal section view of the experimental flume

Fig. 1 A longitudinal section view of the experimental flume

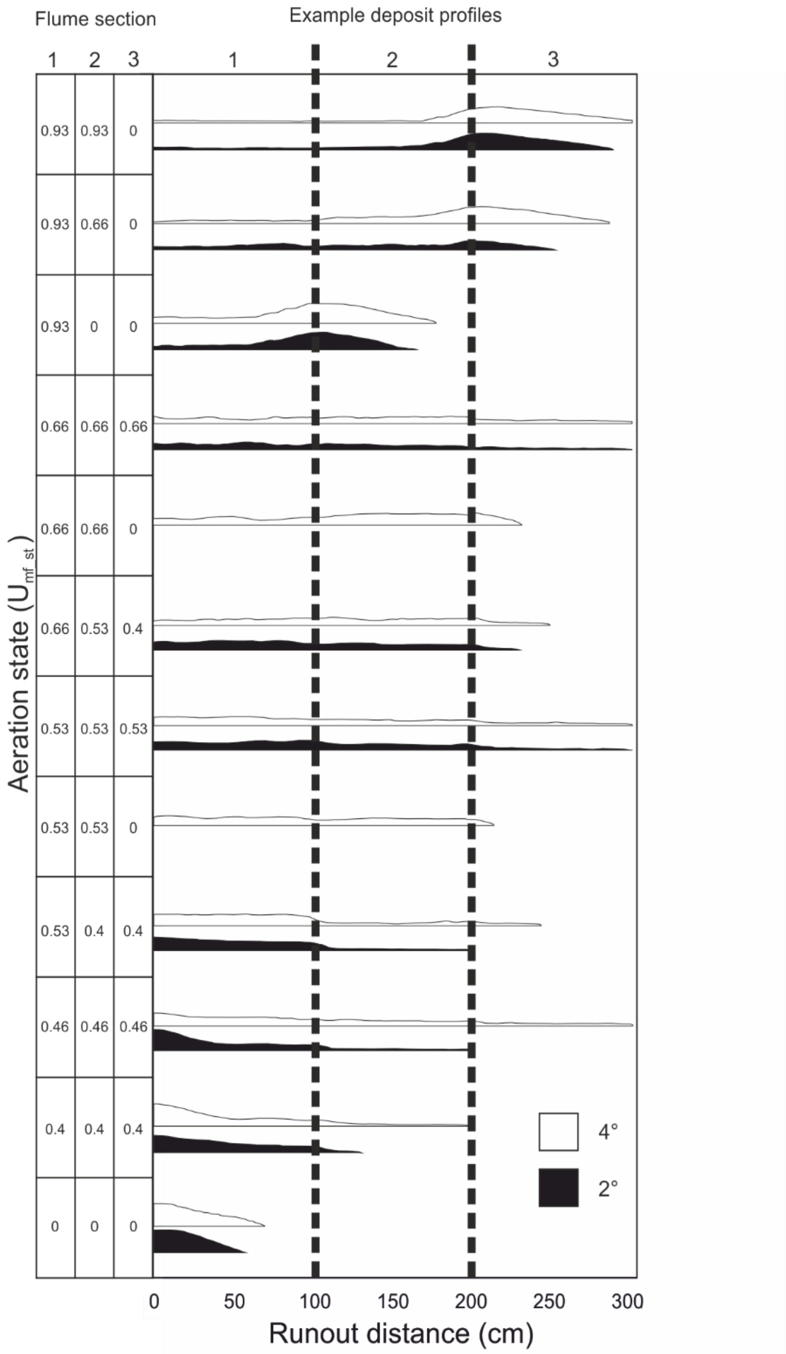

Fig. 2 Runout distances for various aeration states on different slope angles. Bars are shown as profiles of the actual deposits formed. Aeration states of the three chambers are given on the y-axis. Dividing lines show the transition points between the three chambers. Flume length is 300 cm. Vertical scale = horizontal scale

Fig. 2 Runout distances for various aeration states on different slope angles. Bars are shown as profiles of the actual deposits formed. Aeration states of the three chambers are given on the y-axis. Dividing lines show the transition points between the three chambers. Flume length is 300 cm. Vertical scale = horizontal scale

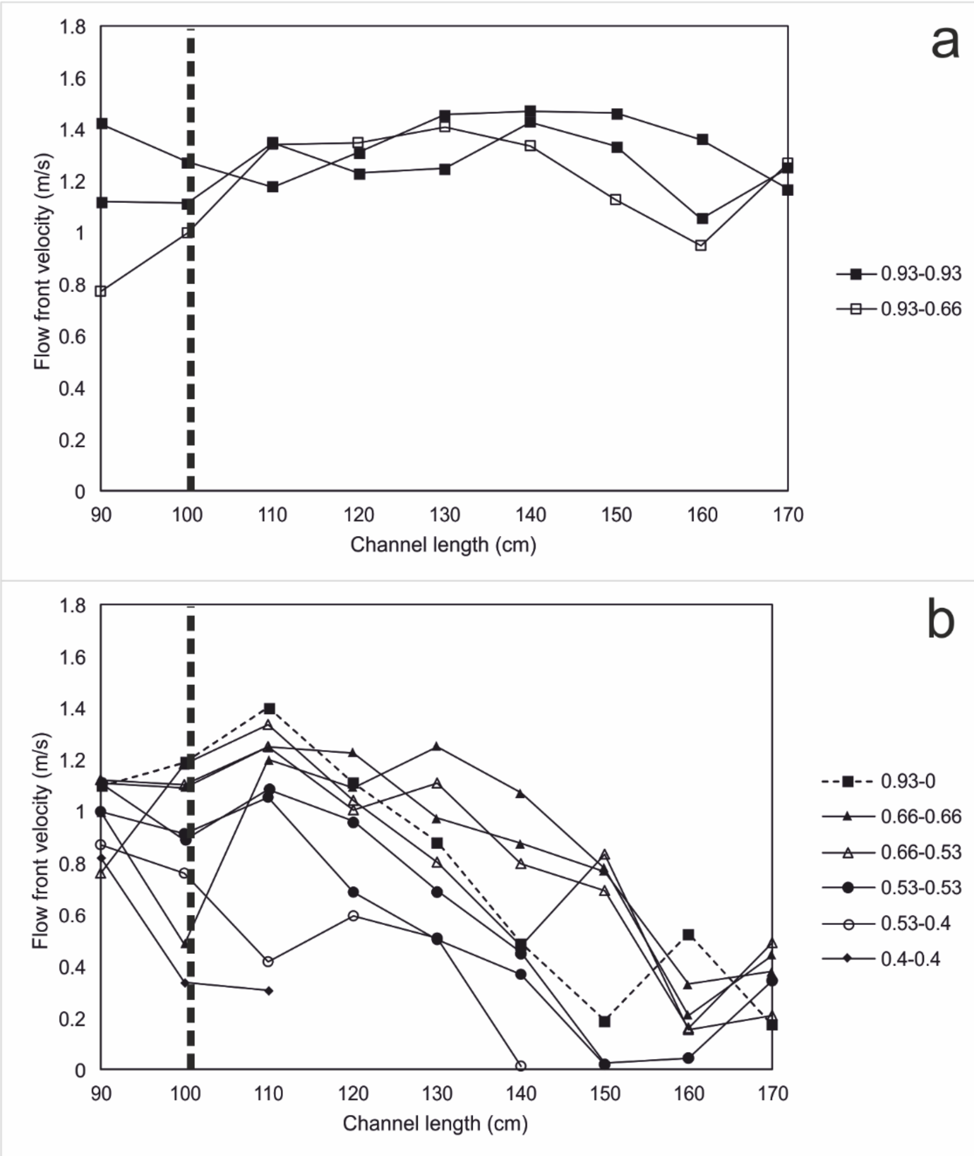

Fig. 3 Plots showing flow front velocity as each flow propagates past the distance intervals 0.8-1.7 m, with a 4° channel slope. Note that where a profile stops on the x-axis this does not necessarily mean the flow has halted, in some cases it represents where the flow front has become too thin to accurately track. Dividing line shows the transition between the first and second chamber along the flume. The aeration states (in U_{mf_st}) of a flow in the first two chambers are shown on the right hand side of each plot. **a** shows flows which experience a high uniform or near-uniform gas supply from chamber 1 into chamber 2, whereas **b** shows flows which experience a low uniform gas supply, or a lower gas supply into chamber 2 than chamber 1, encouraging de-aeration

Fig. 3 Plots showing flow front velocity as each flow propagates past the distance intervals 0.8-1.7 m, with a 4° channel slope. Note that where a profile stops on the x-axis this does not necessarily mean the flow has halted, in some cases it represents where the flow front has become too thin to accurately track. Dividing line shows the transition between the first and second chamber along the flume. The aeration states (in U_{mf_st}) of a flow in the first two chambers are shown on the right hand side of each plot. **a** shows flows which experience a high uniform or near-uniform gas supply from chamber 1 into chamber 2, whereas **b** shows flows which experience a low uniform gas supply, or a lower gas supply into chamber 2 than chamber 1, encouraging de-aeration

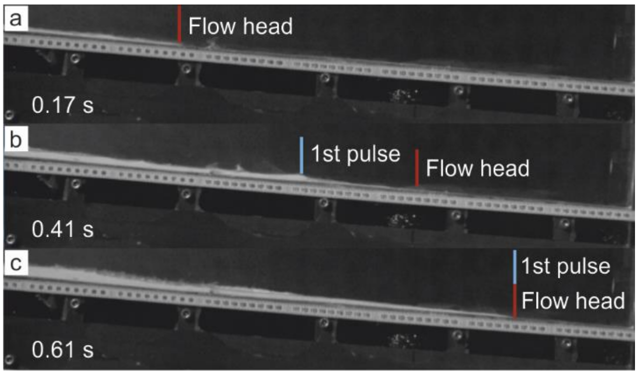

Fig. 4 High-speed video frames of an experimental flow on a 4° slope under 0.93-0-0 U_{mf_st} conditions (**Fig. 2**). Numbers on left are time in seconds since the flow front entered the frame. **a** The front of the flow enters the frame. **b** The flow front continues to run out as the first flow pulse catches and begins to override it. **c** The flow front is completely overtaken by the first pulse. See video (Online Resource 1)

Fig. 4 High-speed video frames of an experimental flow on a 4° slope under 0.93-0-0 U_{mf_st} conditions (**Fig. 2**). Numbers on left are time in seconds since the flow front entered the frame. **a** The front of the flow enters the frame. **b** The flow front continues to run out as the

first flow pulse catches and begins to override it. **c** The flow front is completely overtaken by the first pulse. A video of this experiment is presented in Online Resource 1

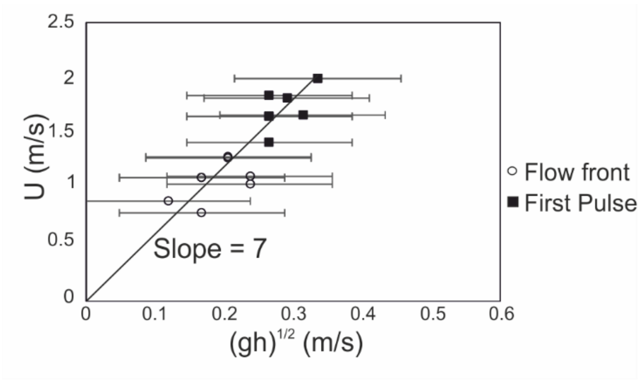

Fig. 5 Froude number *Fr = U/(gh)*$^{1/2}$ for the flow fronts and first pulses of selected experimental flows. Uncertainties in velocity are smaller than the size of the symbols. Uncertainties in flow height are relatively large due to the thinness of the flow fronts relative to video resolution.The best fit gives *Fr = 7*

Fig. 5 Froude number $Fr = \frac{U}{(gh)^{1/2}}$ for the flow fronts and first pulses of selected experimental flows. Uncertainties in velocity are smaller than the size of the symbols. Uncertainties in flow height are relatively large due to the thinness of the flow fronts relative to video resolution. The best fit gives *Fr* = 7

Proportion of U_{mf_st}	Gas velocity (cm/s)
1.00	0.83
0.93	0.77
0.66	0.55
0.53	0.44
0.46	0.38
0.4	0.33

Table 1 Conversion of gas velocities used in the experiments into proportions of U_{mf_st} (0.83 cm/s

Deposit population	Flow conditions	Aeration State (U_{mf_st})	Example profile
Thick downstream wedge	Large aeration decrease	0.93-0.93-0 0.93-0-0 0.93-0.66-0 (4°)	
Even thickness but thin in third chamber	Uniform aeration	0.66-0.66-0.66 0.53-0.53-0.53 0.46-0.46-0.46 (4°)	
Even thickness	Moderate – low aeration decrease	0.93-0.66-0 (2°) 0.66-0.66-0 0.53-0.53-0 0.66-0.53-0.4	
Centre of mass inside first chamber	Low uniform aeration	0.53-0.4-0.4 0.4-0.4-0.4 0.46-0.46-0.46 (2°)	
Flat-topped wedge	Unaerated	0-0-0	

Table 2 Populations of deposit types and the aeration states and slope angles which form them

Sample	Run	x(50%) (µm)	Mean (µm)	Sqrd diff	Variance	Std Dev
1	1	64.39		0.256711		
	2	63.16	63.88333	0.523211	0.275622	0.524997
	3	64.1		0.046944		
2	1	65.44		0.3481		
	2	65.62	66.03	0.1681	0.5054	0.710915
	3	67.03		1		
3	1	59.93		3.6481		
	2	62.58	61.84	0.5476	1.854867	1.361935
	3	63.01		1.3689		
4	1	58.24		0.603211		
	2	58.66	59.01667	0.127211	0.671622	0.819526
	3	60.15		1.284444		
5	1	53.38		11.04454		
	2	49.66	50.05667	0.157344	6.589089	2.566922
	3	47.13		8.565378		
6	1	48.42		9.221344		
	2	44.34	45.38333	1.088544	4.761089	2.181992
	3	43.39		3.973378		
7	1	65.42		0.2304		
	2	65.68	64.94	0.5476	0.755467	0.869176
	3	63.72		1.4884		
8	1	69.08		1.314844		
	2	67.37	67.93333	0.317344	0.657489	0.810857
	3	67.35		0.340278		

Table 3 Grain size data and statistics for the particles used in the experiments. Six samples were taken from across the material batch and subjected to particle size analysis using a QICPIC